Marten, F. B., Rodrigues, S., Benjamin, O. J., Terry, J. R., & Richardson, Mar, P. (2008). Onset of poly-spike complexes in a mean-field model of human EEG and its application to absence epilepsy.

Early version, also known as pre-print

Onset of poly-spike complexes in a mean-field model of human EEG and its application to absence epilepsy.

By Frank Marten, Serafim Rodrigues, Oscar Benjamin, Mark P. Richardson(*) and John R. Terry

Department of Engineering Mathematics, University of Bristol, Bristol, BS8 1TR
(*) Institute of Psychiatry, King's College London, Camberwell, SE5 8AF

In this paper we introduce a modification of a mean-field model used to describe the brain's electrical activity as recorded via Electroencephalography (EEG). The focus of the present study is to understand the mechanisms giving rise to dynamics observed during absence epilepsy, one of the classical generalized syndromes. A systematic study of data from a number of different subjects with absence epilepsy demonstrates a wide variety of dynamical phenomena in the recorded EEG. In addition to the classical spike and wave activity, there may be poly-spike and wave, wave-spike or even no discernible spike-wave onset during seizure events. The model we introduce is able to capture all of these different phenomena and we describe the bifurcations giving rise to these different types of seizure activity. We argue that such a model may provide a useful clinical tool for classifying different sub-classes of absence epilepsy.

Keywords: Absence Epilepsy, spike-wave, human EEG, mathematical modelling, bifurcations

1. Introduction

Epilepsy is the commonest serious primary brain disease affecting 380,000 people in the UK, with 30,000 new cases per year. Epilepsy carries significant mortality (Cockerell *et al.* 1994) and morbidity (Buck *et al.* 1994) as well as reduced quality of life (Devinsky *et al.* 1995). A recent National Sentinel Audit revealed an annual mortality in the UK of >2000 cases per year. Epilepsy has high costs, estimated at £1.93billion per year in the UK in 1994 (Cockerell *et al.* 1994). The focus of the present paper is on a class of primary generalized seizures, called absence seizures, which typically affect children and young adolescents. The term 'absence' arises from the clinical presentation of these seizures whereby cognitive abilities are lost, often resulting in brief periods of behavioural arrest (or absences). When monitoring subjects with epilepsy using electroencephalography (EEG), dynamically evolving patterns may be observed in cortical electrical activity; the classical pattern associated with absence seizures is an approximately 3Hz spike and wave discharge that is synchronous across all channels of activity. However, closer inspection of EEG recorded from different subjects (for example Hrachovy & Frost 2006) demonstrates a number of different dynamical phenomena, for example poly-spike and wave discharges and wave-spike discharges, in addition to the classical spike-wave profile (see Figure 1). Previous theoretical work by Breakspear *et al.* (2006),

Rodrigues *et al.* (2006) and Rodrigues *et al.* (2007), has focussed on understanding the transitions from healthy states to the classical spike and wave discharge, demonstrating that oscillatory behaviour (the wave part of the complex) arises as a result of a Hopf bifurcation upon increasing excitatory connections between cortex and thalamus. Further increasing this parameter, gives rise to the spike due to the appearance of an inflection point in the vector field. In addition, these previous studies have demonstrated the predictive and descriptive validity of a mean-field approach for modelling a wide range of healthy states as well as generalized seizures in humans (Breakspear *et al.* 2006). Studies of EEG recordings collected during absence seizures lend themselves naturally to this approach, since during an absence seizure there exists a hypersynchronous state that entrains populations of neurons to the same dynamic activity.

In the present work, we introduce a mean-field model of cortico-thalamic interactions and examine mechanisms by which transitions from healthy states to those observed from a number of different absence seizures can occur. Two model parameters are indicated to be crucial in this respect. One is the parameter that governs the strength of excitatory cortical-thalamic interactions, which has been demonstrated to be crucial in our previous studies. The other parameter is a time-delay that we introduce to describe the different time-scales of interactions for GABA_A and GABA_B receptors in the specific relay nuclei. We demonstrate that this delay is crucial in determining the number of spikes per cycle during seizure activity in the model and that the excitatory coupling plays a role in the transition from healthy to seizure dynamics. It is natural to consider such interactions as several human and animal studies of absence seizures have implicated abnormalities in cortico-thalamic loops in the generation of seizure activity (Crunelli & Leresche 2002).

Our work is motivated by a desire to elucidate potential mechanisms for the onset of seizure activity which could in turn inform novel experimental and clinical approaches to studying epilepsy, for example the potential to develop seizure prediction algorithms based on bifurcation tracking of parameters of interest that could provide an alternative approach to the standard one based on signal processing (see Mormann *et al.* 2005 for a review).

2. Clinical data

The data presented in this paper came from a database of 48 seizures from 20 subjects, who were part of a consecutive series having absence seizures during routine outpatient EEG investigation. EEG data were obtained using conventional clinical equipment (mention make and model of each EEG system and sampling rates here). Standard silver-silver chloride disk electrodes attached to the scalp were used, and electrode placement followed the Maudsley variant of the international 10-20 system. EEG recordings typically lasted about 1 hour, with periods of wakefulness with eyes open and closed, as well as drowsiness and sleep in some patients. Attempts were made in all cases to provoke seizures using hyperventilation and photic stimulation (stroboscopic stimulation at a range of frequencies). All EEG data were reviewed by a trained Clinical Encephalography Technician, who identified spike-wave discharges for further analysis here.

In addition to EEG data, medical records were reviewed to establish the epilepsy syndrome according to the classification of the International League Against Epilepsy

(1989). In each case, patients were assigned to one of the four syndromes: childhood absence epilepsy, juvenile absence epilepsy, juvenile myoclonic epilepsy, generalised tonic-clonic seizures on awakening. Althought these syndromes are clearly-defined in terms of age of onset, other seizure types experienced by the patient and other clinical criteria, there is considerable overlap between these syndromes. Although absence seizures are seen more often in children than adults, persistent of absence epilepsy from childhood into adulthood is well-recognised, as is de novo adult-onset (Trinka 2005). The patients studied here had an age range 3 to 65.

A typical absence is a non-convulsive epileptic seizure. It consists of a sudden, brief impairment of consciousness accompanied by a generalized, synchronous, bilateral, 2.54-Hz spike and slow-wave discharge seen on EEG, and followed by abrupt recovery (Crunelli & Leresche 2002). Typical absence seizures occur in several different idiopathic generalised epilepsy syndromes, and detailed phenomena during the absence seizure may vary between syndromes and between patients, for example in duration and accompanying motor features such as myoclonic jerks of limbs or eyelids. The ictal EEG usually shows a single spike followed by a wave, but may show polyspikes. The discharges are traditionally regarded as synchronous across all channels and usually bilateraly symmetrical. Typically the spike-wave discharge frequency is highest at the start of the burst and falls through the seizure. As well as interindividual variability in EEG and in clinical presentation, there is considerable variability in response to drug treatment (Duron *et al.* 2005).

3. Mathematical description

(*a*) *The mean-field model*

In order to model EEG-activity from patients with absence seizures, we investigate neural dynamics in two distinct brain regions, namely the thalamus and the cerebral cortex. The motivation for this approach is that thalamocortical interactions are found to play an essential role in the generation of this (poly)spike-wave EEG-activity. A variety of experimental evidence is summarized in section 8.1 of Destexhe & Sejnowski (2001). The model that we present may be thought of as a mean-field, neural-mass model. It describes the dynamics of large interacting groups of neurons, which are referred to as neural masses. The model arises as a result of merging a number of theoretical viewpoints:

1. The pioneering work of Lopes da Silva *et al.* (1974) and Freeman (1975), who developed equations of motion, describing the behaviour of neural masses, based upon detailed experimental studies.

2. Differences in the time scales of activation / inactivation due to $\mathrm{GABA}_{A/B}$ receptors in the thalamus as described in Figures 5.8 and 5.9 in the book of Destexhe & Sejnowski (2001).

3. Incorporation of the cortico-thalamic loop, shown in studies (Destexhe & Sejnowski 2001) to be important in the generation of sleep spindles and abnormal seizure activity.

4. The wave-like equation for the propagation of cortical activity, as described by Jirsa & Haken (1996).

Merging these approaches together, we consider an extension of an existing mean-field approach, employed in previous studies (Breakspear *et al.* 2006 and Rodrigues *et al.* 2006), consisting of both cortical and thalamic components. The thalamic component is assumed to consist of two neural masses; an excitatory mass of specific relay nuclei (s), and an inhibitory mass of reticular nuclei (r). Similarly, the cortical component incorporates both a mass of excitatory pyramidal cells (e) and inhibitory interneurons (i).

Each of the neural masses (e,i,s,r) is described by three dynamical variables: its average membrane potential $V_a(\mathbf{r},t)$, the average firing rate $\varsigma_a(\mathbf{r},t)$ and the axonal field $\phi_a(\mathbf{r},t)$ at position $\mathbf{r}$ and time t. The subscript (a) is used to refer to each of the different masses. These variables obey the following dynamical rules:

$$\left[\frac{1}{\alpha\beta}\frac{\partial^2}{\partial t^2}+\big(\frac{1}{\alpha}+\frac{1}{\beta}\big)\frac{\partial}{\partial t}+1\right]V_a(\mathbf{r},t)=P_a(\mathbf{r},t), \tag{3.1}$$

$$\varsigma_a(\mathbf{r},t)=\frac{Q_a^{max}}{1+exp\big(-\frac{\pi}{\sqrt{3}}\frac{V_a(\mathbf{r},t)-\theta_a}{\sigma}\big)}, \tag{3.2}$$

$$\left[\frac{\partial^2}{\partial t^2}+2\gamma_a\frac{\partial}{\partial t}+\gamma_a^2-\nu_a^2\nabla^2\right]\phi_a(\mathbf{r},t)=(\gamma_a^2-\gamma_a\frac{\partial}{\partial t})\varsigma_a(\mathbf{r},t). \tag{3.3}$$

Equation (3.1) describes changes in the average membrane potential V_a of a neural mass, under incoming post-synaptic potentials P_a. Secondly, equation (3.2) describes the average firing rate of the mass. If V_a exceeds a threshold θ_a, the neural mass fires action potentials with an average rate ς_a. The sigmoidal shape of ς_a ensures that the firing rate never exceeds a maximum value Q_a^{max}. This is crucial, because real neurons cannot fire infinitely quickly. A third equation (3.3), describes propagation of action potential-fields ϕ_a via axons of the neural mass. Axonal fields influence other neural masses via synaptic connections, hence they can lead to new post-synaptic potentials $P(\mathbf{r},t)$.

In Figure 2, we present a schematic of all the connections within the mean-field model. We view the cortex as one compartment, with axonal connections to and from the two thalamic subcompartments. Excitatory connections via fields ϕ_e, ϕ_s are displayed as arrows, while inhibitory connections ϕ_r are given by lines with dots. Specific relay nuclei also receive sensory input ϕ_n, which is modeled as a constant field in our research. Incoming synaptic fields ϕ_a, received by each compartment, are assumed to be linearly summed in the dendritic tree (Robinson *et al.* 2002), hence:

$$P_a(\mathbf{r},t)=\sum_b \nu_{ab}\phi_b(\mathbf{r},t), \tag{3.4}$$

for neural mass (a), where ν_{ab} are coupling constants for the average strength of synaptic connections, which closes the set of rules of the mean-field model.

A further change from previous studies is the nature of the delay. In the present work, we are motivated by the studies of Destexhe & Sejnowski (2001) and introduce two connections ϕ_r(t) and ϕ_r(t - τ) from reticular nuclei to specific relay nuclei. These connections are designed to represent inhibitory GABA_A and GABA_B synapses. Since GABA_B functions via second messenger processes, its post-synaptic currents develop on a slower time scale than the currents of GABA_A (Figures 5.8 and 5.9 in Destexhe & Sejnowski 2001). Hence, we expect that if thalamic neurons

fire, the $GABA_B$ mediated connection to specific relay nuclei will be delayed with respect to $GABA_A$. In research by Coombes *et al.* (2002), a similar delay was obtained as follows: the wave-like equation (3.3) is derived from an integral between the firing rate $\varsigma_a(\mathbf{r}, t)$ and a synaptic kernel. Depending on the particular synapse modeled, this integral can lead to a delay in the right-hand side of equation (3.3). Combining this with equation (3.4), and the computations in appendix A, gives a delayed connection ϕ_r(t - τ).

In summary, equations (3.1-3.4) are the theoretical framework of our research. Since such a large system of DDEs is computationally expensive, it is desirable to make some simplifications. First of all, cortical inhibitory interneurons are relatively sparce compared to pyramidal cells (a ratio of 4:1 in favour of pyramidal cells). Excitatory (e) neurons are believed to be the main source of EEG, hence we approximate $V_i \approx V_e$ and $\varsigma_i \approx \varsigma_e$ (Robinson *et al.* 2002). Furthermore, γ_a represents a ratio between an axonal velocity, and a typical length scale for axonal propagations. Since inhibitory neurons only have short range projections, compared to excitatory neurons (Robinson *et al.* 1997, 2002), we effectively have $\gamma_{i,r} \to \infty$. A similar argument, explained in Rodrigues *et al.* (2008), can be used to approximate $\gamma_s \to \infty$.

In Robinson *et al.* (2002), it is shown that removing the time-derivative in the right-hand side of (3.3) does not influence the numerical results, hence it can be dropped for all neural masses. If we combine this with $\gamma_{i,r,s} \to \infty$, equation (3.3) reduces to $\phi_{i,r,s} = \varsigma_{i,r,s}$. Excitatory cortical neurons (e) can not be approximated this way. However, because we model a generalized seizure, with global cortical activity, we neglect the spatial dependence of fields and voltages in our model. The above approximations reduce our model to a system of 8 first order delay differential equations, given in appendix A. By making this reduction, our model becomes computationally more tractable.

(*b*) *Numerical methods*

Large systems of delay differential equations, like our model (A.2), can produce a variety of complex dynamics. In our case, we are especially interested in 2-4Hz periodic solutions, which resemble EEG-activity during absence seizures. First of all, numerical integrators can be used to obtain time series of the model (A.2). The results can be qualitatively compared to EEG-traces of patients. Numerical integration is performed through a fourth order Adams-Bashforth scheme, adjusted to model delay differential equations (Baker *et al.* 1994).

Secondly, since we wish to understand the onset, change and termination of absence seizure dynamics, and in particular the onset and termination of (poly)spike patterns, we employ the Matlab package DDE-BIFTOOL (Engelborghs *et al.* 2001) to find and continue branches of these solutions, as parameters of the model are varied. A further package PDDE-CONT (Szalai 2005) is also used in instances where continuing branches of periodic solutions becomes intractable using Matlab.

4. Results

Our results are presented in two sections: In the first section, we demonstrate that the mean-field model can produce periodic patterns that closely resemble EEG-

data recorded during human absence seizures. We considered a database of 48 seizures and observed that as well as the classical single spike and wave per cycle, the dynamics in many seizures consisted of multiple (poly)spikes per cycle. We illustrate that in the model, the formation of spikes occurs as a result of inflection-points in the solutions of our mean-field equations. Moreover, the existence of these inflection-points can be studied using one-parameter bifurcation diagrams.

We extend these results in the second section, using the numerical continuation packages described previously to track bifurcations and the birth of inflection-points in our model. This generalizes our previous analysis by providing a detailed understanding of the mechanisms leading to the onset and deformation of (poly)spike patterns. We proceed to link these results back to time-series data simulated from the model and draw a comparison between the model and clinical data from our absence seizure database.

(*a*) *EEG and Model: time series and bifurcations*

Previous research relating mean-field models and absence seizures has focused on reproducing single spike and wave patterns (Breakspear *et al.* 2006, Rodrigues *et al.* 2006), an example of which is given in Figure 1(a), that are classically associated with absence seizures. More general polyspike patterns, such as the ones displayed in Figure 1(b,c), have been studied in only limited cases (Wendling *et al.* 2002). Our aim is to build on this research, and explain the mechanisms that cause the onset of such polyspike activity, which we observe frequently in our absence seizure database. The approach we follow extends the earlier research of Rodrigues *et al.* (2006). In this work it was shown that the coupling strength ν_{se}, between pyramidal cells in the cortex and specific cells in the thalamus, is a crucial parameter for observing the onset of spike-wave activity.

As the model we consider is a modification of that considered in these earlier studies, our starting point will also be to focus on the parameter ν_{se}, with the main variable of interest being $\phi_e(t)$. We recall that this variable describes the axonal fields of cortical pyramidal cells, which give the main contribution to EEG-signals. Hence, we assume a functional relation between ϕ_e and the scalp EEG-voltage, which to first approximation may be considered linear. However, we stress that even in this simple case, the constant of proportionality is patient specific.

Bifurcation diagrams provide a systematic way to study the dynamics of $\phi_e(\mathrm{t})$. Here, the aim is to find qualitative changes in ϕ_e under variations of the parameter ν_{se}, for example, transitions from 'healthy' steady-state neuronal activity to 'seizure' (poly)spike-wave patterns. We construct the diagrams by integrating the system of delay equations (A.2) as described in section 3. During the integration, all model parameters are kept fixed to the values in Table (1). Once finished, we add a small increment δ to the value of ν_{se}. Equations (A.2) are then integrated again, with the previous solution as initial condition. This procedure is repeated hundreds of times. During each step, we record the local maxima and minima of $\phi_e(\mathrm{t})$ and plot them against ν_{se}. For the GABA_B coupling, we choose a delay $\tau = 100\,\mathrm{ms}$. This represents the order of magnitude of rise and decay-time of GABA_B currents (Destexhe & Sejnowski 2001, Figures 5.8 and 5.9). The bifurcation diagram is shown in Figure 3(a).

The dynamics we find are similar to past investigations (Rodrigues *et al.* 2006).

For $\nu_{se} < 1.48 \times 10^{-3}$ V s we observe that the system (A.2) resides in a steady-state. Thus all of its eight variables are constant in time including $\phi_e(\mathrm{t})$. This can be compared to clinical EEG-data before the seizure occurs, see arrows from Figure 3(a) to (b). Under normal conditions EEG signals are noisy patterns around a steady state average voltage. At $\nu_{se} \approx 1.48 \times 10^{-3}$ V s we find the onset of a $\sim$3Hz oscillation, through a Hopf-bifurcation. The emanating two curves in the diagram represent its local maxima and minima. Some patients develop similiar oscillatory EEG-signals at the onset of absence seizures (Rodrigues *et al.* 2006). Their patterns do not contain any spikes and just consist of $\sim$3Hz sine-like oscillations.

An interesting change is observed at $\nu_{se} \approx 1.66 \times 10^{-3}$ V s. It seems like $\phi_e(\mathrm{t})$ undergoes a second bifurcation at this point. However, a closer look at the time series reveals that the solution developed a small local maximum, through an inflection point. An example is sketched in Figure 3(c). This maximum develops into the familiar spike, which characterizes spike-wave patterns. This is by no means a period doubling bifurcation; the stability and period of the solution do not change along $\nu_{se} \approx 1.66 \times 10^{-3}$ V s. Rather, this point represents a local deformation of the periodic solution profile (Rodrigues *et al.* 2008). We term this a 'ghost-bifurcation', since it mimics the shape of a bifurcation in our diagram.

Ghost-bifurcations have been observed in past research (Rodrigues *et al.* 2006, Figure 1), where the classification of the solution was left undetermined. The diagrams in these investigations always displayed at most one single ghost-bifurcation, which led to the classic spike-wave profiles. An interesting new feature of our present model is the occurence of a second ghost-bifurcation at $\nu_{se} \approx 1.8 \times 10^{-3}$ V s. This corresponds to the appearance of a double spike-wave solution. In real patient EEG, such patterns can also develop during an absence seizure (arrow to Figure 3(b)). Based on these observations, we wish to address the following questions: how many spikes can appear in the solutions of our model? Is their existence related the delayed GABA_B coupling? And what happens to $\phi_e(\mathrm{t})$ as ν_{se} is increased further?

(*b*) *Continuation in two parameters*

The analysis presented in the previous section has demonstrated that the coupling between cortex and specific, ν_{se}, is a crucial parameter in this model. Increases in ν_{se} lead to the onset of seizure dynamics, as well as transitions from single spike and wave to polyspike solutions. Recent numerical studies of mean-field models of the general form presented in this paper have demonstrated that the delay τ also plays a crucial role in the observance of spikes. For example, in the absence of the delay only a transition to oscillatory behaviour via a Hopf bifurcation was observed, without spikes arising (Rodrigues *et al.* 2008). Similarly, we do not observe spikes arising in time-series produced from the model for values of $\tau < 0.04$ suggesting that the delay is again significant in the generation of spike and wave solutions. To investigate this further, we employ two parameter continuation, where we study ν_{se} and the delay τ simultaneously. This method allows us to draw 2-dimensional curves of (ghost)bifurcations in a (ν_{se}, τ) parameter plane.

These diagrams, also known as activity-maps, are extremely important. The bifurcation curves are boundaries between different dynamical regions of the model, such as 'healthy' regions, where the model exhibits steady-state solutions, and 'seizure' regions, where the model produces polyspike patterns. In previous re-

search (Wendling *et al.* 2002), similar activity-maps were obtained by simulating EEG-activity on a two-parameter grid. We extend this method using the numerical continuation-tools discussed in section 2. This technique is more useful for creating activity-maps, since finding the boundaries of a parameter-region is more efficient than finding the entire region step by step and calculates the boundary to a higher resolution. We also wish to find curves of ghost-bifurcations in the (ν_{se}, τ)-plane. Standard continuation methods are not appropriate in this case as the branch of solutions here does not correspond to a standard bifurcation. To overcome this, we employ a special detection-method to find inflection points (this approach was first used in Rodrigues *et al.* 2008).

Figure 4 shows the activity maps obtained. Panel (a) displays various bifurcation curves, computed for our mean-field model (A.2). In panel (b), we performed the same computation for the original corticothalamic model, which has been discussed in the works of Breakspear *et al.* (2006) and Rodrigues *et al.* (2006, 2008). Exemplars of the solution profiles produced by each model demonstrate the need to consider modifications of the model. In the original model, although multiple inflection points exist they do not develop into spikes as is the case for the model studied in this paper (which we return to in due course). The main difference between the two approaches is the incorporation of the delay τ. Whereas we propose in the present study a delay to describe the slow $GABA_B$-synapse, the model in (b) assumed that the delay arises due to synaptic transmission times for signals travelling between cortex and thalamus.

In both panels we find a single curve of Hopf-bifurcations (HB) and various ghost-bifurcations, given by solid black curves. We also find period doubling (PD) and saddle node bifurcations of limit cycles (SL), given by dashed and solid red curves respectively. Their significance will be discussed below. Different regions in Figure 4, bounded by (ghost)bifurcations, are marked by various shades of blue. The Hopf-curves define the transition from the model's steady state (lightest blue) into periodic solutions (darker blue). In both Figures, we find that an increase in delay τ leads to a decrease in the value of ν_{se} at the Hopf-bifurcation (HB). Thus if the delay in both models is increased, a weaker coupling strength ν_{se} is required to initiate oscillatory behaviour. If τ is decreased below $\tau \simeq 0.04$ in panel (a) or $\tau \simeq 0.02$ in panel (b), we end up in a region where both models do not support spike-wave solutions.

Other features of Figure 4(a) and (b) are qualitatively different; in panel (a) we find a clear relation between the GABA_B delay τ and the number of spikes observed. An increase of τ leads to a stepwise increase of the number of spikes. The spiking regions are separated by black curves of ghost-bifurcations. Crossing such a curve means that a spike is added or removed from the model-solution. Conversely, panel (b) displays a different scenario. There exists a region of spike waves between $\nu_{se} \approx 3.8 \times 10^{-3}$ V s and $\nu_{se} \approx 6.2 \times 10^{-3}$ V s. Around $\tau \approx 0.08$ s, another region labeled "2 Spike-wave" exists, bounded by a curve of ghost-bifurcations. The solution $\phi_e(\mathrm{t})$ contains a wave, followed by a small spike, a plateau of constant ϕ_e, and a larger spike. A similar region can be seen at ($\nu_{se} = 3 \times 10^{-3}, \tau = 0.16$). The original corticothalamic model is mainly capable of qualitatively reproducing single spike-wave solutions.

If τ is fixed and ν_{se} is increased in Figure 4, eventually one of the red branches will be crossed. This implies that the (poly)spike solutions either lose stability via a

period doubling bifurcation (PD) or vanish completely in a saddle-node bifurcation (SL). A detailed analysis of the period doubling bifurcations in Figure 4(b) is given in the recent work of Rodrigues *et al.* (2008). It was found that small isles of stable periodic solutions and small chaotic regions exist, on the right of the (PD)-curve. We have found similar dynamics in panel (a). These small regions of more complex dynamics are beyond the scope of the present study and remain under investigation.

How can we relate the activity-map in Figure 4(a) back to time-series of our mean-field model? Figure 5 provides a schematic overview. Panels (a1-c1) consist of two parts: the top part is a small section taken from Figure 4(a). Below each section, we display a bifurcation diagram in ν_{se}. As an example, in panel (a1), we display a subsection of Figure 4(a) around $\tau = 0.06\,\mathrm{s}$. Hence, if the delay of the slow GABA_B coupling is fixed at 0.06 s, and we increase ν_{se} stepwise, the diagram in the lower part of (a1) is obtained. In all panels (a1-c1), $\phi_e(\mathrm{t})$ develops into periodic 2-4 Hz (poly)spike patterns, which eventually destabilize via saddle-node (SL) or period doubling (PD) bifurcations. The latter bifurcation occurs in a tiny window of parameter-space, and is followed by an even tinier chaotic attractor. These features could only be captured by DDE-BIFTOOL and not our numerical integrator. Past the (SL) and (PD) points, $\phi_e(\mathrm{t})$ then converges to a steady state $\phi_e = 250\,\mathrm{s}^{-1}$. This steady state, which coexists with all the periodic solutions of our model, corresponds to the maximal neuronal firing-rate at $\varsigma_a = Q_a^{max}$.

Some of the various periodic (poly)spike patterns of $\phi_e(\mathrm{t})$ are given in Figure 5 (a2-c2). For example, the time series in panels (a2) correspond to a fixed connection-delay $\tau = 0.06\,\mathrm{s}$, and from top to bottom, $\nu_{se} = 0.0017$, 0.002 and $0.0024\,\mathrm{V\,s}$. Similarly, panels (b2) and (c2) correspond to $\tau = 0.10\,\mathrm{s}$ and $\tau = 0.16\,\mathrm{s}$, where $\nu_{se} = 0.0017$, 0.002, $0.0026\,\mathrm{V\,s}$ and $\nu_{se} = 0.0016$, 0.00165, $0.002\,\mathrm{V\,s}$ from top to bottom respectively. These time series correspond to sections of the bifurcation diagrams in panels (a1-c1). We find that an increase of GABA_B delay not only results in more spikes, but also a decrease in frequency. At $\tau = 0.06$ we find patterns with a frequency of approximately 3 Hz. For $\tau = 0.10$ and $\tau = 0.16$ the frequency decreases to 2.3Hz and 1.8Hz respectively. The first two frequencies lie in the range of absence-seizure EEG, of which the main frequency-component is situated between 2 and 4Hz respectively.

Our final step is, to make a link between the above mentioned time series, and real patient EEG-data. Some examples are shown in Figure 6. In section 3 we pointed out that ϕ_e can be approximated to be linearly related to EEG-voltages. An often used convention, is that the constant of proportionality is taken to be negative (Robinson 2005). Column (a) shows EEG traces from our seizure database, taken from 3 different patients with childhood absence epilepsy. Column (b) displays various time-traces of our model, using the activity map in Figure (4) to determine parameter regimes. In each case we find an interesting qualitative agreement between model and data, suggesting that there is significant variation in the value of the delay τ between patients. It remains an important question to interpret the biophysical meaning of such a variation.

5. Discussion

The work presented in this paper was motivated by a desire to understand the mechanisms responsible for transitions between different types of seizure activity

observed in EEG recordings from human subjects with absence seizures. Studying a database of 48 seizures from 20 subjects, we observed not only the classical single spike and wave activity, but a wide variety of polyspike and wave solutions (up to three spikes per cycle). Building on our earlier work in this area (Breakspear *et al.* 2006, Rodrigues *et al.* 2006) we isolated the transition to single spike and wave activity, identifying an inflection point in the system dynamics as causing the spike in the model (Rodrigues *et al.* 2008). Subsequently we investigated the addition of further spikes per cycle, but observed that successive inflection points occurring in the original model of Robinson *et al.* (2002) did not accurately reproduce data recordings from human subjects (see Figure 4(b)).

Consequently we developed a modified cortico-thalamic model, which incorporated differences in GABAergic channels in the connections between inhibitory and excitatory thalamic neuronal populations. Studying the transitions in this model, using a combination of bifurcation theory and numerical continuation methods, we were able to map out in (ν_{se}, τ)-space branches of inflection points giving rise to different numbers of spikes per cycle. These activity maps demonstrate that the delay plays a crucial role in these transitions. A Hopf bifurcation was observed to give a transition between healthy activity and oscillatory behaviour preceding the onset of spike and wave activity. From the analysis of the model we were able to obtained time-series from our model that mimics those recorded from human subjects (Figure 5). In this regard a further important question is to understand the mechanisms that control the frequency of oscillations within each window corresponding to solutions with different numbers of spikes. We are currently investigating this phenomena and the results will be presented elsewhere.

These findings also suggest a number of hypotheses of potential clinical relevance that should be investigated. First the onset of the seizure in our model corresponds to the transition between steady-state and oscillatory activity, rather than the onset of spike-wave behaviour. This suggests that clinical symptoms of absence seizures may occur before the observation of spike-wave activity in EEG recordings. This could potentially be investigated using a continuous performance task in human subjects with absence seizures, such as following a moving trace on a screen. Secondly, the variation in delay between patients as observed when fitting model time-series to data, suggests that it is important to establish a mapping between macroscopic models and microscopic parameters. Finally, the techniques presented here provide a means for predicting when a seizure might occur, by estimating and tracking parameters of the model implicated in seizure onset from clinical data. Techniques for the tracking of bifurcations from experimental data have recently been proposed and validated in an electronic circuit by Sieber and Krauskopf (2008) and techniques based on this approach may have validity in this case. This would provide an alternative method for seizure prediction then more traditional methods based on signal processing (Mormann *et al.* 2005).

6. Acknowledgments

All authors acknowledge financial support from the EPSRC via Grant EP/D068436/01 and the Leverhulme Trust via the Theoretical Neuroscience Network. Useful conversations with Gabor Stepan are also gratefully acknowledged.

A. The delay model

We briefly illustrate how our mean field model is derived, using the theory and approximations in section 3. Recall that we model 4 neural masses (e,i,s,r), described by the laws in equations (3.1-3.3) and the connection scheme in Figure 2, which should be combined with equation (3.4).

The following simplifications have been made: we neglect any spatial dependence, hence the Laplacian in equation (3.3) vanishes for all neural masses, and consequently V_a, ϕ_a, ς_a only depend on time. In addition, we neglect the time-derivative in the right-hand side of this equation. The local approximations $\gamma_{i,s,r} \approx 0$ reduce equation (3.3) to $\phi_{i,s,r}(\mathrm{t}) = \varsigma_{i,s,r}(\mathrm{t})$. We point out that excitatory cortical neurons (e) cannot be approximated in this way, hence their fields ϕ_e follow:

$$\frac{1}{\gamma_e^2}\left[\frac{\partial^2}{\partial t^2} + 2\gamma_e\frac{\partial}{\partial t} + \gamma_e^2\right]\phi_e(t) = \varsigma_e(t). \tag{A.1}$$

For convenience, we assume that the firing rates $\varsigma_a(\mathrm{t})$ of all 4 neural masses have the same parameters, hence we omit the (a)-labels in Q_a^{max}, θ_a and σ_a, and write $\varsigma_{e,i,s,r}(\mathrm{t}) = \varsigma(V_{e,i,s,r}(\mathrm{t}))$.

We reduce our model further, by assuming the symmetry $V_i = V_e$. This allows us to neglect the voltage variable V_i alltogether, and write the field $\phi_i = \varsigma(V_e(\mathrm{t}))$. Using all these approximations, we have effectively 4 variables left: the 3 voltages $V_{e,s,r}(\mathrm{t})$ and the excitatory cortical field $\phi_e(\mathrm{t})$. The voltages follow equation (3.1), while the field $\phi_e(\mathrm{t})$ follows equation (A.1). The variables are coupled together via equation (3.4) and the scheme in Figure 2. Because of the second order derivatives, we can rewrite our model as an 8-dimensional first order system.

We point out that the difference in $\mathrm{GABA}_{A,B}$ synapses from reticular (r) to specific relay (s) neurons are modeled via a time delay. Thus, neural mass (s) receives a post-synaptic potential $P_s = \nu_{se}\phi_e(t) + \nu_{sn}\phi_n(t) + \nu_{sr}^A\phi_r(t) + \nu_{sr}^B\phi_r(t-\tau)$. Combining this with all other approximations, the final model becomes:

$$\left\{\begin{array}{lcl}
\frac{\mathrm{d}}{\mathrm{d}t}\phi_e(t) &=& y(t),\\
\frac{\mathrm{d}}{\mathrm{d}t}y(t) &=& \gamma_e^2\left[-\phi_e(t) + \varsigma(V_e(t))\right] - 2\gamma_e y(t),\\
\frac{\mathrm{d}}{\mathrm{d}t}V_e(t) &=& z(t),\\
\frac{\mathrm{d}}{\mathrm{d}t}z(t) &=& \alpha\beta\left[-V_e(t) + \nu_{ee}\phi_e(t) + \nu_{ei}\varsigma(V_e(t)) + \nu_{es}\varsigma(V_s(t))\right] - (\alpha+\beta)z(t),\\
\frac{\mathrm{d}}{\mathrm{d}t}V_s(t) &=& w(t),\\
\frac{\mathrm{d}}{\mathrm{d}t}w(t) &=& \alpha\beta\left[-V_s(t) + \nu_{sn}\phi_n + \nu_{se}\phi_e(t) + \nu_{sr}^A\varsigma(V_r(t)) + \nu_{sr}^B\varsigma(V_r(t-\tau))\right],\\
& & -(\alpha+\beta)w(t),\\
\frac{\mathrm{d}}{\mathrm{d}t}V_r(t) &=& v(t),\\
\frac{\mathrm{d}}{\mathrm{d}t}v(t) &=& \alpha\beta\left[-V_r(t) + \nu_{re}\phi_e(t) + \nu_{rs}\varsigma(V_s(t))\right] - (\alpha+\beta)v(t).
\end{array}\right. \tag{A.2}$$

Table 1. *Parameter values for the model*

Quantity	Description	Value
θ	Threshold of membrane potential, before cell fires.	0.015 V
σ	Standard deviation of firing rate.	0.006 V
Q_{max}	Average maximum firing rate.	250 s^{-1}
γ_e	Average ratio between pulse velocity and axon range.	100 s^{-1}
α	Receptor offset time constant.	50 s^{-1}
β	Receptor offset time constant.	200 s^{-1}
τ	Time delay, due to slow $GABA_B$ synapse.	varies
ν_{sn}	Subthalamic coupling strength.	20e-4 V s
ν_{ee}	Excitatory corticocortical coupling strength.	10e-4 V s
ν_{ei}	Inhibitory corticocortical coupling strength.	-18e-4 V s
ν_{es}	Specific thalamic to cortical coupling.	17e-4 V s
ν_{se}	Cortical to specific thalamic coupling.	varies
$\nu_{sr}^{A,B}$	$GABA_{A,B}$ thalamic relay to specific thalamic coupling.	-8e-4 V s
ν_{re}	Cortical to thalamic relay nuclei coupling.	0.5e-4 V s
ν_{rs}	Specific thalamic to thalamic relay coupling.	5e-4 V s

References

Baker, C. T. H., Paul, C. A. H. & Wille, D. R. 1994 Issues in the numerical solution of evolutionary delay differential equations. Report no. 248, Department of Mathematics, University of Manchester.

Breakspear, M., Roberts, J. A., Terry, J. R., Rodrigues, S., Mahant, N. & Robinson, P. A. 2006 A Unifying Explanation of Generalized Seizures Through Nonlinear Brain Modeling and Bifurcation Analysis. *Cereb. Cortex* **16**, 1296–1313.

Buck, D., Baker, G. A., Jacoby, A., Smith, D. F. & Chadwick, D. W. 1997 Patients' experiences of injury as a result of epilepsy. *Epilepsia* **38**, 439–444.

Commission on Classification and Terminology of the International League Against Epilepsy. 1989 Proposal for revised classification of epilepsies and classification of epilepsies and epileptic syndromes. *Epilepsia* **30**, 389399.

Cockerell, O. C., Johnson, A. L., Sander, J. W., Hart, Y. M., Goodridge D. M. & Shorvon, S. D. 1994 Mortality from epilepsy: results from a prospective population-based study. *Lancet* **344**, 918–921.

Coombes, S., Lord, G. J. & Owen, M. R. 2002 Waves and bumps in neuronal networks with axo-dendritic synaptic interations. *Physica D* **178**, 219–241.

Crunelli, V. & Leresche, N. 2002 Childhood absence epilepsy: genes, channels, neurons and networks. *Nat Rev Neuro* **3**, 371-382.

Destexhe, A. & Sejnowski, T.J. 2001 *Thalamocortical Assemblies* OUP.

Devisnky, O., Vickrey, B. G., Cramer, J., Perrine, K., Hermann, B., Meador, K. & Hays, R. D. 1995 Development of the quality of life in epilepsy inventory. *Epilepsia* **36**, 1089–1104.

Duron, R. M., Medina, M. T., Martnez-Juarez, I. E., Bailey, J. N., Perez-Gosiengfiao, K. T., Ramos-Ramrez, R., Lopez-Ruiz, M., Alonso, M. E., Ortega, R. H. C., Pascual-Castroviejo, I., Machado-Salas, J., Mija, L. & Delgado-Escueta, A. V. 2005 Seizures of idiopathic generalized epilepsies. *Epilepsia* **46**, 34–47.

Engelborghs, K., Luzyanina, T. & Samaey, G. 2001 DDE-BIFTOOL v. 2.00: a Matlab package for bifurcation analysis of delay differential equations, Report no. TW-330, Department of Computer Science, K.U. Leuven.

Freeman, W. J. 1975 *Mass action in the nervous system. Examination of the neurophysiological Basis of Adaptive behaviour through the EEG* Academic Press New York.

Hrachovy, R. A. & Frost Jr., J. D. 2006 The EEG in selected generalized seizures. *J. Clin. Neurophysiol.* **23**, 312–332.

Jirsa, V. K. & Haken H. 1996 Field Theory of Electromagnetic Brain Activity. *Phys. Rev. Lett.* **77**, 960–963.

Lopes da Silva, F. H., Hoeks, A., Smits H. & Zetterberg L. H. 1974 Model of brain rhythmic activity. *Kybernetic* **15**, 27–37.

Mormann, F., Kreuz, T., Rieke, C., Andrzejak, R., Kraskov, A., David, P., Elger, C. & Lehertz, K. 2005 On the predictability of epileptic seizures. *Clin. Neurophys.* **116**, 569–587.

Robinson, P.A., Rennie, C. J. & Wright, J. J. 1997 Propagation and stability of waves of electrical activity in the cerebral cortex. *Phys. Rev. E* **56**, 826–840.

Robinson, P.A., Rennie, C. J. & Rowe, D. L. 2002 Dynamics of large-scale brain activity in normal arousal states and epileptic seizures. *Phys. Rev. E* **65**, 041924.

Rodrigues, S., Terry, J. R. & Breakspear, M. 2006 On the genesis of spike-wave activity in a mean-field model of human thalamic and corticothalamic dynamics. *Phys. Lett. A* **355**, 352-357.

Rodrigues, S., Goncalves, J. & Terry, J. R. 2007 Existence and stability of limit cycles in a macroscopic neuronal population model. *Physica D* **233**, 39–65.

Rodrigues, S., Barton, D., Szalai, R., Benjamin, O., Richardson, M. P. & Terry J. R. 2008 Transitions to spike-wave oscillations and epileptic dynamics in a human cortico-thalamic mean-field model. Preprint, University of Bristol.

Suffczynski, P., Lopes da Silva, F. H., Parra, J., Velis, D. & Kalitzin, S. 2005 Epileptic transitions: Model predictions and experimental validation. *J. Clin. Neurophys.* **22**, 288–299.

Szalai, R. 2005 PDDE-CONT: A continuation and bifurcation software for delay-differential equations. Department of Applied Mechanics, Budapest University of Technology and Economics.

Trinka, E. 2005 Absences in adult seizure disorders. *Acta Neurol Scand* **112**, (Suppl 182) 12–18.

Wendling, F., Bartolomei, F., Bellanger, J. J. & Chauvel, P. 2002 Epileptic fast activity can be explained by a model of impaired GABAergic dendritic inhibition. *Eur. J. Neurosci.* **15**, 1499–1508.

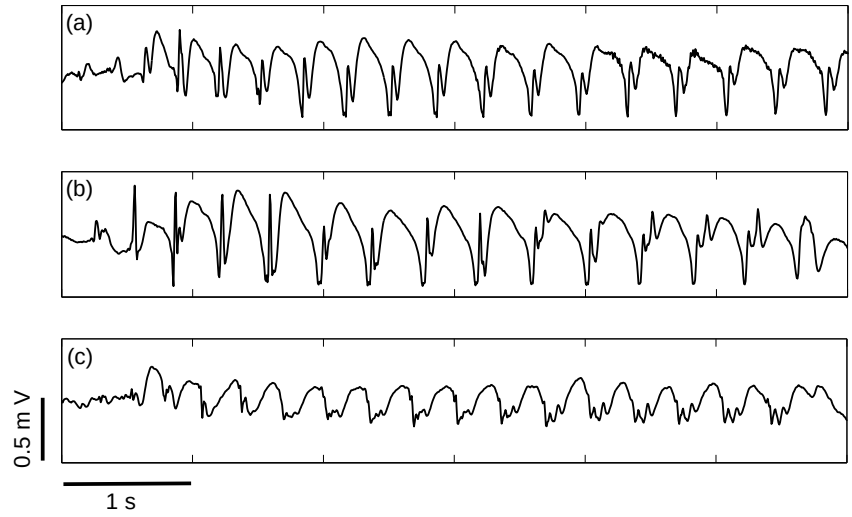

Figure 1. *EEG-recordings of 3 different patients with childhood absence epilepsy (CAE); (a) A typical spike-wave oscillation. (b) During a seizure, the EEG-profile can show additional spikes. (c) A similar EEG-recording as in (b). We again observe a polyspike-wave pattern, however it is difficult to discern whether the spikes are leading the wave or vice-versa.*

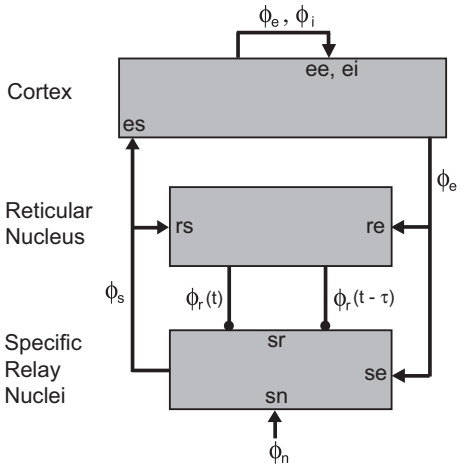

Figure 2. *Overview of the corticothalamic model. Neuronal populations consist of e=excitatory cortical; i=inhibitory cortical; s=specific relay and r=reticular nuclei. Populations s and r are coupled by a fast $GABA_A$ and a slow $GABA_B$ connection, the latter is indicated by* $(t - \tau)$.. Synaptic weights between populations of different types are represented by *ee*, *re* etc.

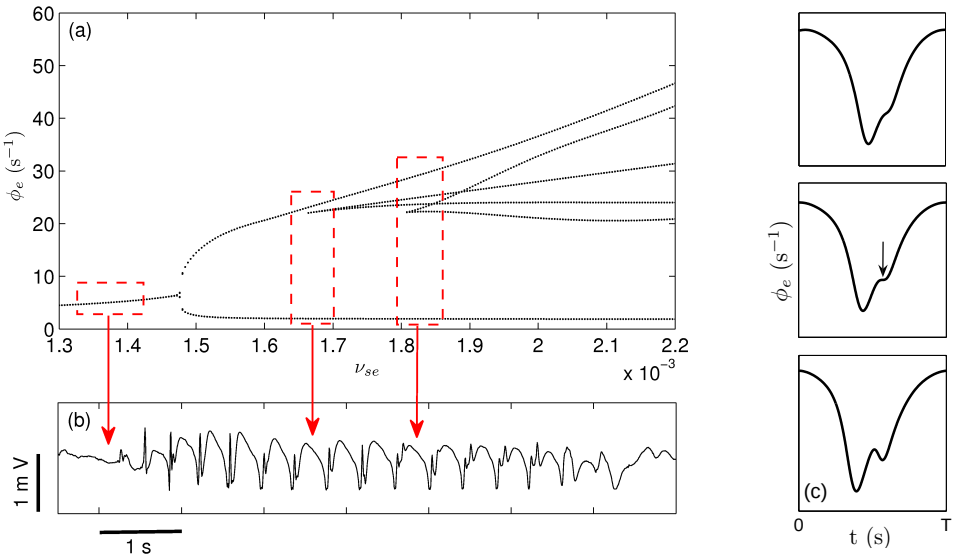

Figure 3. *(a) Bifurcation-diagram in ϕ_e, obtained by varying the cortex-to-thalamus coupling parameter ν_{se}. (b) The onset of a seizure from Human EEG-data. Whilst the arrows between panel (a) and (b) are not meant for direct comparison of the bifurcation diagram and EEG, we stress that qualitative features of the diagram can be found in real patient data. This suggests that ramping up the parameter ν_{se} is responsible for the transition to seizures in the model. (c) The onset of a spike-wave occurs through an inflection-point (arrow). We term this point "ghost bifurcation", note that it does not change the stability or period of the solution.*

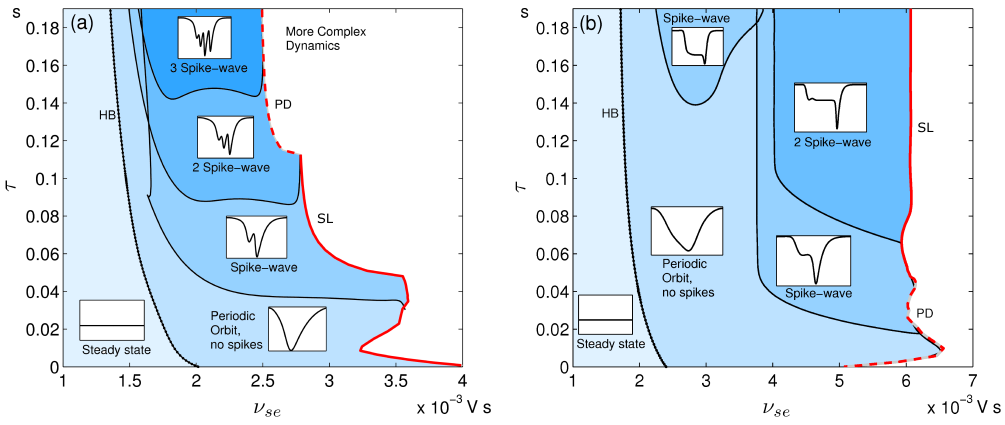

Figure 4. *Illustrating two-parameter continuation performed in the (ν_{se},τ)-plane. Panel (a) shows the results for the cortico-thalamic model considered in this paper. As a comparison, we present the same plot for the original model considered in Breakspear et al. (2006) in panel (b). In both cases, transitions from steady-state to periodic orbits are mediated by a curve of Hopf-bifurcations (HB). Subsequently orbits can develop spikes via inflection points (black-curves), that eventually turn unstable via period-doubling (PD) or disappear in saddle-node bifurcations of limit cycles (SL), see red dashed and red solid curves. Notice that the solution profiles in the original model do not replicate the polyspike solutions observed in the clinical data.*

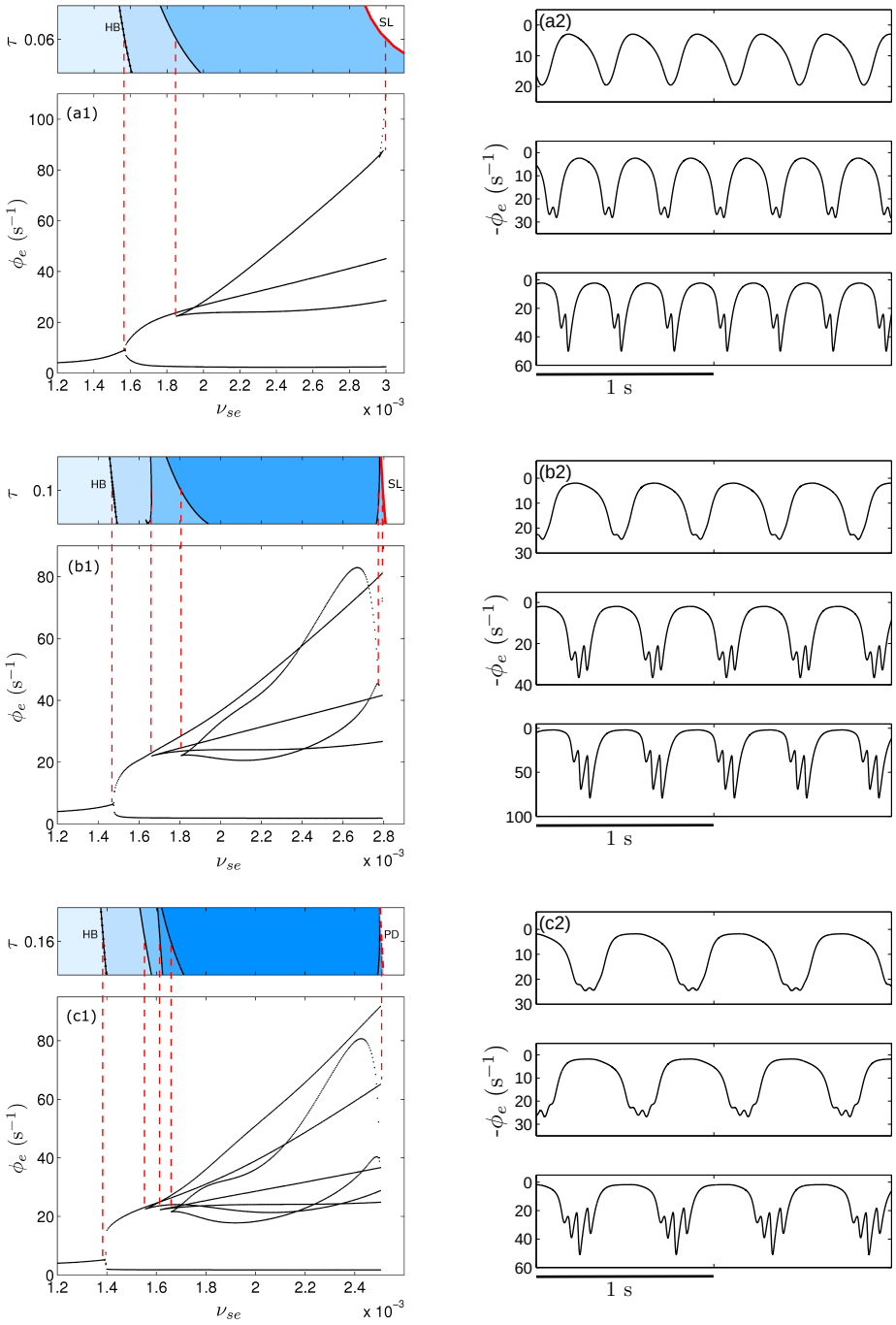

Figure 5. *Panels (a1-c1) display a comparison between two-parameter continuation from Figure 4(a) and one-parameter bifurcation diagrams in ν_{se}. From top to bottom, the values of τ in these diagrams are 0.06, 0.10 and 0.16 s respectively. Panels (a2-c2) display time series of our model. They correspond to the one-parameter diagrams in (a1-c1), and are computed for fixed values of ν_{se}. From top to bottom, ν_{se} =0.0017, 0.002 and 0.0024 V s; ν_{se} = 0.0017, 0.002, 0.0026 V s and ν_{se} =0.0016, 0.00165, 0.002 V s respectively.*

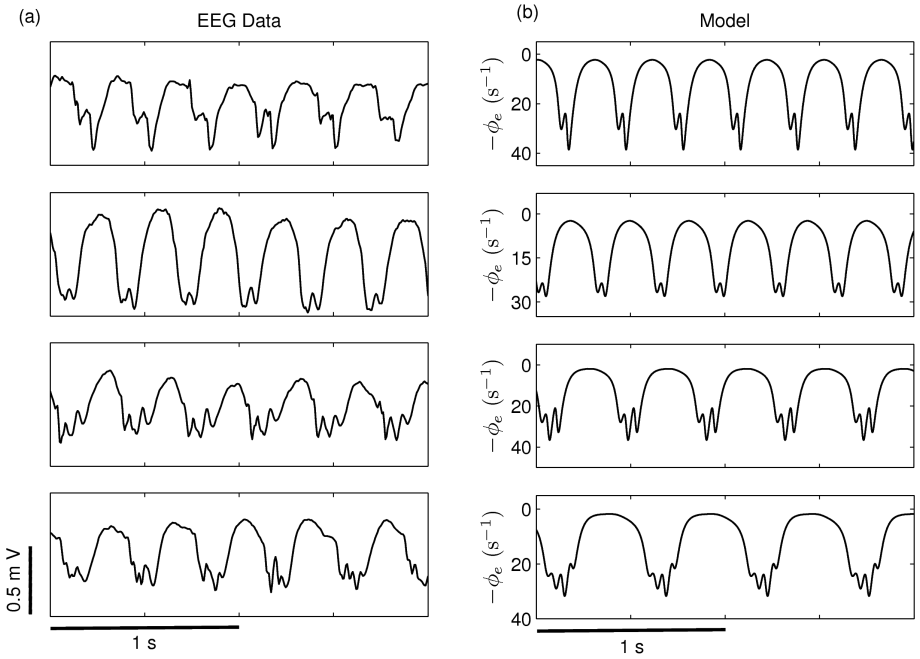

Figure 6. *A qualitative comparison between human EEG-data and our corticothalamic model. Column (a) contains EEG-recordings from 4 different patients with an absence seizure. From top to bottom, the first 3 patients are diagnosed with childhood absence epilepsy (CAE), while the patient in the lower panel is diagnosed with juvenile absence epilepsy (JAE). Column (b) displays time series from our model.*